第 34 卷第 12 期 无 机 化 学 学 报 Vol.34 No.12
2018 年 12 月 CHINESE JOURNAL OF INORGANIC CHEMISTRY 2280-2290

基于单–和双–三唑衍生物的三个 Cu(Ⅱ)和 Cu(Ⅰ)多金属氧簇基配合物的水热合成及光催化性能

刘媛媛*,[1,2] 李欣书[1] 张慧敏[1] 丁 斌[1,2]
([1]无机–有机杂化功能材料化学教育部重点实验室,天津师范大学化学学院,天津 300387)
([2]南京大学配位化学国家重点实验室,南京 210093)

摘要: 在水热条件下,利用多齿的单–和双–三唑衍生物,制备了 3 种基于多金属氧簇基(POM)的 Cu(Ⅱ)和 Cu(Ⅰ)杂化材料,即{[Cu(L_1)$_2$(Mo_4O_{13})]·2H_2O}$_n$ (**1**),{[$Cu_{1.5}$(L_2)(HL_2)(H_2O)(Mo_4O_{13})]·2H_2O}$_n$ (**2**),{[Cu_2(L_3)$_{1.5}$(Mo_4O_{13})]·H_2O}$_n$ (**3**)(L_1=4-pyridine-2-1,2,4-triazole,HL_2=3-(4*H*-1,2,4-triazol-4-yl)benzoic acid,L_3=*trans*-4,4′-azo-1,2,4-triazole)。通过单晶 X 射线衍射、傅里叶变换红外光谱和粉末 X 射线衍射分析确定了它们的结构。在 **1** 中,$Mo_4O_{13}^{2-}$阴离子和 Cu(Ⅱ)中心通过双齿 L_1 相互连接,最终形成了二维(2D)POMs 基的 Cu(Ⅱ)杂化金属–有机骨架。在 **2** 中,$Mo_4O_{13}^{2-}$阴离子和 Cu(Ⅱ)中心通过桥接水原子(O18),双齿 HL_2 和三齿 L_2^-相互连接,最终形成了三维(3D)POMs 基的 Cu(Ⅱ)微孔金属–有机骨架。在 **3** 中,L_3 配体桥接相邻的 Cu(Ⅰ)中心和 $Mo_4O_{13}^{2-}$阴离子,最终形成独特的双重穿插结构的 3DPOMs 基的 Cu(Ⅰ)杂化配位框架。光催化实验研究表明,样品 **1**~**3** 对于不同有机染料罗丹明 B (RhB)、亚甲基蓝(MB)和甲基橙(MO)都具有很好的光催化降解能力。

关键词: 三唑; Cu(Ⅱ); Cu(Ⅰ); 多金属氧簇; 光催化
中图分类号: O614.121 **文献标识码**: A **文章编号**: 1001-4861(2018)12-2280-11
DOI:10.11862/CJIC.2018.274

Three Polyoxometalate-Based Cu(Ⅱ) and Cu(Ⅰ) Coordination Polymers with Mono- and Bis-triazole Derivatives: Hydrothermal Assembly and Photocatalytic Properties

LIU Yuan-Yuan*,[1,2] LI Xin Shu[1] ZHANG Hui-Min[1] DING Bin[1,2]
([1]*Key Laboratory of Inorganic-Organic Hybrid Functional Material Chemistry, Ministry of Education, College of Chemistry, Tianjin Normal University, Tianjin* 300387, *China*)
([2]*State Key Laboratory of Coordination Chemistry, Nanjing University, Nanjing* 210093, *China*)

Abstract: Three novel polyoxometalate (POM)-based Cu(Ⅱ) and Cu(Ⅰ) hybrid materials with multi-dentate mono- and bis-triazole derivatives, namely {[Cu(L_1)$_2$(Mo_4O_{13})]·2H_2O}$_n$ (**1**), {[$Cu_{1.5}$(L_2)(HL_2)(H_2O)(Mo_4O_{13})]·2H_2O}$_n$ (**2**), {[Cu_2(L_3)$_{1.5}$(Mo_4O_{13})]·H_2O}$_n$ (**3**) (L_1=4-pyridine-2-1,2,4-triazole, HL_2=3-(4*H*-1,2,4-triazol-4-yl)benzoic acid,L_3=*trans*-4,4′-azo-1,2,4-triazole) have been designed and synthesized by hydrothermal method. The structures of **1**~**3** have been determined by single crystal X-ray diffraction, FT-IR infrared spectra and powder X-ray diffraction analyses. In **1**, $Mo_4O_{13}^{2-}$ anions and Cu(Ⅱ) centers are inter-linked by bidentate L_1, which are arranged into 2D POMs-based Cu(Ⅱ) hybrid metal-organic framework. In **2**, $Mo_4O_{13}^{2-}$ anions and Cu(Ⅱ) centers are inter-linked via bridging aqua atoms (O18), bi-dentate HL_2 and tri-dentate L_2^-, which are arranged into 3D POM-based Cu(Ⅱ) micro-porous metal-organic framework. In **3**, L_3 ligands bridge neighboring Cu(Ⅰ) centers and $Mo_4O_{13}^{2-}$ anions, which ultimately forms unique two-fold interpenetrating 3D POM-based Cu(Ⅰ) hybrid coordination framework. Photocatalytic activities for

收稿日期:2018-08-06。收修改稿日期:2018-09-26。
国家自然科学基金(No.21301128),天津市自然科学基金(No.14JCQNJC05900),天津市高等学校创新团队培养计划(No.TD12-5038)和天津师范大学大学生创新训练项目(No.201612)资助。
*通信联系人。E-mail:hxxylyy@mail.tjnu.edu.cn

decomposition of different organic dyes of rhodamine B (RhB), methylene blue (MB) and methyl orange (MO) have been investigated for **1**~**3**, indicating that **1**~**3** are good candidates for photocatalytic degradation of the organic dyes. CCDC: 1474258, **1**; 1477985, **2**; 1544278, **3**.

Keywords: triazole; Cu(Ⅱ); Cu(Ⅰ); polyoxometalate; photocatalytic

0 Introduction

In recent years, the inorganic-organic coordination polymers have become a unique class of functional materials because of their unique chemical applications and beautiful structural motifs[1]. Polyoxometalates (POMs), defined as metal-oxide clusters based on polyanions, have received intensive attention because of their many important applications in electrical conductivity, catalysis, medicine, magnetism, materials science, and biological chemistry[2]. As illustrated in the previous literature, some important applications are mainly based on the following reasons: (i) polyoxometalates can be employed as electron and proton reservoirs; (ii) their molecular properties are extremely variable such as shape, size, acidity and charge [3]. Recently, many remarkable works about preparing the desired metal-organic frameworks (MOFs) are the utilization of the polyanions coordination ability to bind with versatile transition-metal organic units, which have been presented in coordination polymers[4-6]. This synthetic strategy can bring the merits of each row-material together, such as intriguing structural motifs, good physical and chemical properties[7].

For the rational design and preparation of the POM-based coordination frameworks, judicious selective of organic linkers is quite important. The organic linkers can be divided into two parts: pre-synthesized and *in-situ* synthesized linkers[8]. The former have been widely utilized in the POM-based reaction systems, including Nitrogen-donor linkers, poly-carboxylate linkers and so on[9]. Among the Nitrogen-containing heterocyclic organic linkers, 1,2,4-triazole and its derivatives are intriguing because the linkers combine the coordination geometries of both imidazoles and pyrazoles due to their three heteroatoms arrangement. For instance, the organic linkers have been utilized to construct the open MOFs, which contain unsaturated metal clusters and possess even framework flexibility and high thermal stability[10-11]. As depicted in Scheme 1, the multi-dentate mono- and bis-triazole derivatives, namely 4-pyridine-2-1,2,4-triazole (L_1), 3-(4*H*-1,2,4-triazol-4-yl)benzoic acid (HL_2) and *trans*-4,4′-azo-1,2,4-triazole (L_3), which can afford strong coordination nitrogen donors and carboxylate donors to metal centers. It can be anticipated that L_1, HL_2 and L_3 can be utilized as multi-dentate coordination donors to coordination metallic centers, which can further construct many novel inorganic-organic POM-based hybrid materials[12].

Previously we also began to explore the coordination chemistry and functional application of Nitrogen-containing heterocyclic ligands and its derivatives[13-16]. In this work under hydrothermal conditions, three

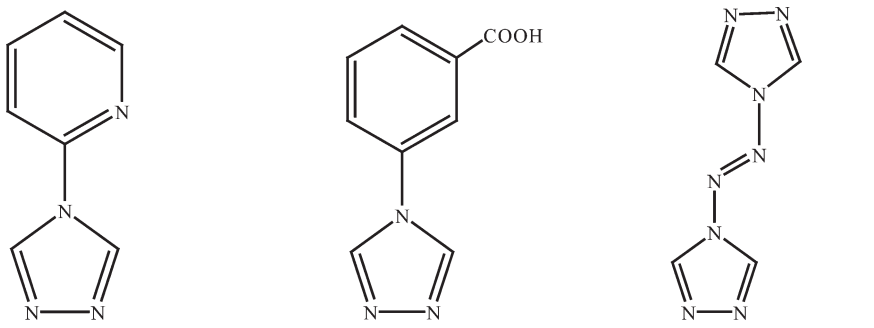

4-pyridine-2-1,2,4-triazole (L_1)　3-(4*H*-1,2,4-triazol-4-yl)benzoic acid (HL_2)　*trans*-4,4'-azo-1,2,4-triazole (L_3)

Scheme 1　Three multi-dentate 1,2,4-triazole derivative ligands L_1, HL_2 and L_3

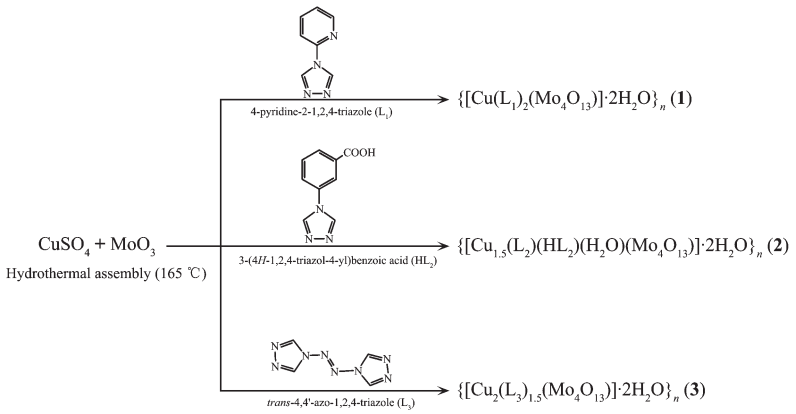

Scheme 2 Hydrothermal assembly of a series of Cu(Ⅱ) and Cu(Ⅰ) hybrid polyoxometalate-based coordination frameworks

novel polyoxometalate (POM)-based Cu(Ⅱ) and Cu(Ⅰ) hybrid materials with multi-dentate mono- and bis-triazole derivatives, namely $\{[Cu(L_1)_2(Mo_4O_{13})]\cdot 2H_2O\}_n$ (**1**), $\{[Cu_{1.5}(L_2)(HL_2)(H_2O)(Mo_4O_{13})]\cdot 2H_2O\}_n$ (**2**), $\{[Cu_2(L_3)_{1.5}(Mo_4O_{13})]\cdot H_2O\}_n$ (**3**) have been designed and synthesized (Scheme 2). Their crystallographic structures have been determined by single crystal X-ray diffraction, FT-IR infrared spectra and PXRD analyses. Photocatalytic activities for decomposition of different organic dyes, namely rhodamine B (RhB), methylene blue (MB) and methyl orange (MO), have been investigated for **1**~**3**.

1 Experimental

1.1 General

Ligands L_1 (4-pyridine-2-1,2,4-triazole), HL_2 (3-(4*H*-1,2,4-triazol-4-yl) benzoic acid) and L_3 (*trans*-4,4′-azo-1,2,4-triazole) were prepared according to the literature methods[17]. All the other reagents were commercially available and utilized without further purification. Perkin-Elmer 240 elemental analyzer was ulitilized to perform C, H and N microanalyses. Powder X-ray diffraction patterns were determined on a D/Max-2500 X-ray diffractometer using Cu $K\alpha$ radiation (λ=0.154 1 nm, U=40 kV, I=40 mA) with a 2θ range of 5°~50°. A Lamdba 900 UV-Vis-NIR spectroscopy was utilized to measure the UV-Vis diffuse reflectance spectra at the ambident temperature.

1.2 Preparation of coordination complexes 1~3

$\{[Cu(L_1)_2(Mo_4O_{13})]\cdot 2H_2O\}_n$ (**1**). $CuSO_4\cdot 5H_2O$ (75.00 mg, 0.3 mmol), L_1 (43.8 mg, 0.3 mmol) and MoO_3 (57.60 mg, 0.4 mmol) were added in 10 mL deionized H_2O. The mixture were transferred and placed into a Teflon vessel in a steel autoclave, heated at 165 ℃ for 72 h and then cooled to ambient temperature during 24 h. The blue strip-shaped single crystals of **1** were washed by H_2O, aether and air-dried. Elemental analysis Calcd. for $C_{14}H_{12}CuMo_4N_8O_{14.50}$(%): C, 17.31; H, 1.25; N, 11.53. Found(%): C, 17.55; H, 1.35; N, 11.82. FT-IR (cm^{-1}): 3 122(m), 2 615(w), 1 593(m), 1 528(m), 1 470(m), 1 441(m), 1 343(m), 1 253(m), 938(w),912(m), 813(m), 568(m), 476(w).

$\{[Cu_{1.5}(L_2)(HL_2)(H_2O)(Mo_4O_{13})]\cdot 2H_2O\}_n$ (**2**). $CuSO_4\cdot 5H_2O$ (100.00 mg, 0.4 mmol), HL_2 (94.5 mg, 0.5 mmol) and MoO_3 (14.40 mg, 0.1 mmol) were added into 10 mL deionized H_2O. The mixture were transferred and putted into a Teflon vessel, heated at 165 ℃ for 72 h in a steel autoclave and then cooled to ambient temperature during 24 h. The green strip-shaped single crystals of **2** were washed by H_2O, aether and air-dried. Elemental analysis Calcd. for $C_{18}H_{17}Cu_{1.50}Mo_4N_6O_{19.50}$(%): C, 19.50; H, 1.55; N, 7.58. Found(%): C, 19.73; H, 1.63; N, 7.73. FT-IR (cm^{-1}): 3 180(m), 2 629(w), 1 704(m), 1 548(s), 1 459(m), 1 401(s), 1 332(w), 1 270(m), 948(w), 902(m), 820(m), 765(m), 699(m), 552(m), 479(w).

$\{[Cu_2(L_3)_{1.5}(Mo_4O_{13})]\cdot H_2O\}_n$ (**3**). $CuSO_4\cdot 5H_2O$ (125.00 mg, 0.5 mmol), L_3 (49.2 mg, 0.3 mmol) and MoO_3 (28.80 mg, 0.2 mmol) were added in 10 mL deionized H_2O. The mixture were transferred and placed into a Teflon vessel in a steel autoclave, heated at 165 ℃ for 72 h and then cooled to ambient temperature during 24 h. The red block-shaped single crystals of **3** were

washed by H_2O, aether and air-dried. Elemental analysis Calcd. for $C_6H_8Cu_2Mo_4N_{12}O_{14}$(%): C, 7.33. H, 0.82. N, 17.10. Found(%): C, 7.55; H, 0.98; N, 17.36. FT-IR (cm^{-1}): 3 120(bm), 1 513(s), 1 296(s), 1 176(s), 1 100(m), 1 048(m), 1 000(w), 922(m), 804(m), 661(m), 615(m).

1.3 Photo-catalytic measurements of coordination complexes 1~3

The photo-catalytic measurements of coordination polymers **1~3** were evaluated by the degradation of MB, RhB and MO under irradiation utilizing a 200 W high pressure mercury lamp. The photo-catalytic experiments have been measured in a classical method, 5 mg complex **1** or **2** or **3** were suspended in the water solutions containing three organic dyes (10 $\mu mol \cdot L^{-1}$, 10 mL), respectively. The mixture was stirred in the dark for 30 min for the desorption-adsorption equilibrium, then the mixture was transferred and placed under the lighting of Hg lamp (200 W) with continuous stirring. Next, every 20 minutes intervals, aliquots of the mixture samples were extracted and centrifuged. Finally, the sample was analyzed by UV-Vis analytical technique. The photo-catalytic degradation efficiency (D) can be calculated as below:

$$D=(A_0-A_t)/A_0\times100\%$$

where A_t is the absorbance of dye at time t, A_0 represents the initial absorbance of dyes solution.

1.4 X-ray crystallography

Structure measurements of complexes **1~3** were performed on a computer controlled a Bruker SMART Apex Ⅱ CCD diffractometer equipped with graphite-monochromated Mo $K\alpha$ radiation with radiation wavelength of 0.071 073 nm by using the ω-scan technique. The structures were solved by direct methods and refined with the full-matrix least-squares technique using the SHELXS-97 and SHELXL-97 programs[18-19]. Anisotropic thermal parameters were assigned to all non-hydrogen atoms. The organic hydrogen atoms were generated geometrically; the hydrogen atoms of the water molecules were generated geometrically and refined with isotropic temperature factors. Crystal data collection and refinement details for complexes **1~3** are summarized in Table 1. Selected bond lengths and angles for complexes **1~3** are listed in Table 2. Hydrogen bonds analysis was carried out using the PLATON program, all the hydrogen bonds distances and angles are listed in Table 3.

CCDC: 1474258, **1**; 1477985, **2**; 1544278, **3**.

Table 1 Crystal data and structure refinement information for compounds 1~3

	1	2	3
Empirical formula	$C_{14}H_{12}CuMo_4N_8O_{14.50}$	$C_{18}H_{17}Cu_{1.50}Mo_4N_6O_{19.50}$	$C_6H_8Cu_2Mo_4N_{12}O_{14}$
Formula weight	971.61	1 108.45	983.08
Crystal system	Triclinic	Monoclinic	Monoclinic
Space group	$P\bar{1}$	$C2/c$	$P2_1/c$
Temperature / K	296(2)	296(2)	296(2)
a / nm	0.768 10(8)	2.598 7(4)	1.076 47(11)
b / nm	0.819 54(9)	1.705 0(3)	1.078 40(11)
c / nm	1.111 74(12)	1.569 0(2)	1.807 02(19)
α / (°)	104.754(2)		
β / (°)	93.668(2)	115.779(2)	92.782(2)
γ / (°)	100.439(2)		
V / nm^3	0.661 07(12)	6.260 0(16)	2.095 2(4)
Z	1	8	4
F(000)	472	4 276	1 864
D_c / ($Mg \cdot m^{-3}$)	2.468	2.352	3.117
μ / mm^{-1}	2.722	2.650	4.415
Data, restraint, parameter	2 696, 0, 194	6 486, 42, 450	4 264, 12, 343
GOF	1.024	1.077	1.098

Continued Table 1

R_1[a] [$I \geqslant 2\sigma(I)$]	0.025 1	0.044 5	0.044 4
wR_2[a] (all data)	0.088 0	0.130 3	0.087 0

[a] $R_1 = \sum ||F_o|-|F_c|| / |F_o|$, $wR_2 = [\sum w(F_o^2-F_c^2)^2 / \sum w(F_o^2)^2]^{1/2}$.

Table 2 Selected bond lengths (nm) and angles (°) for coordination polymers 1~3

			1		
Cu(1)-O(1)	0.197 1(2)	Cu(1)-O(1)^{i}	0.197 1(2)	Cu(1)-N(2)	0.197 2(3)
Cu(1)-N(2)^{i}	0.197 2(3)	Cu(1)-O(4)^{i}	0.236 7(3)	Cu(1)-O(4)^{ii}	0.236 7(3)
O(1)-Cu(1)-O(1)^{i}	180.0	O(1)-Cu(1)-N(2)	89.12(11)	O(1)-Cu(1)-N(2)^{i}	90.88(11)
O(1)^{i}-Cu(1)-N(2)^{i}	90.88(11)	N(2)-Cu(1)-N(2)^{i}	180.00(15)	O(1)-Cu(1)-O(4)^{i}	95.94(10)
O(1)-Cu(1)-O(4)^{ii}	84.06(10)	N(2)-Cu(1)-O(4)^{i}	92.66(11)	N(2)-Cu(1)-O(4)^{ii}	87.34(11)
O(4)^{i}-Cu(1)-O(4)^{ii}	180.00(15)				
			2		
Cu(1)-N(4)	0.198 8(5)	Cu(1)-O(15)^{i}	0.199 3(4)	Cu(1)-N(1)	0.202 5(5)
Cu(1)-O(1)	0.222 5(4)	Cu(2)-N(2)	0.201 6(5)	Cu(2)-N(2)^{i}	0.201 6(5)
Cu(2)-N(5)	0.205 6(5)	Cu(2)-N(5)^{i}	0.205 7(5)	Cu(2)-O(18)	0.237 4(5)
Cu(2)-O(18)^{i}	0.237 4(5)	Cu(1)-O(12)^{i}	0.193 8(4)		
O(12)^{i}-Cu(1)-O(15)^{i}	94.37(17)	N(4)-Cu(1)-O(15)^{i}	86.90(19)	O(12)^{i}-Cu(1)-N(1)	89.27(18)
N(4)-Cu(1)-N(1)	89.5(2)	O(15)^{i}-Cu(1)-N(1)	174.13(18)	O(12)^{i}-Cu(1)-O(1)	87.15(16)
N(4)-Cu(1)-O(1)	92.29(18)	O(15)^{i}-Cu(1)-O(1)	98.36(18)	N(1)-Cu(1)-O(1)	86.41(17)
N(2)-Cu(2)-N(2)^{i}	180.0	N(2)-Cu(2)-N(5)	90.25(18)	N(2)^{i}-Cu(2)-N(5)	89.75(18)
N(2)-Cu(2)-O(18)	96.32(19)	N(5)-Cu(2)-O(18)^{i}	94.58(19)	N(5)-Cu(2)-O(18)^{i}	85.42(19)
O(18)-Cu(2)-O(18)^{i}	180.00(7)				
			3		
Cu(1)-N(2)	0.193 1(7)	Cu(1)-N(7)^{i}	0.200 1(7)	Cu(1)-O(4)	0.200 4(5)
Cu(1)-O(4)	0.211 2(6)	Cu(2)-N(10)^{ii}	0.202 0(6)	Cu(2)-N(9)	0.207 7(7)
Cu(2)-N(8)^{i}	0.209 0(7)	Cu(2)-N(1)	0.220 8(7)		
N(2)-Cu(1)-N(7)^{i}	116.2(3)	N(2)-Cu(1)-O(4)	128.7(3)	N(7)^{i}-Cu(1)-O(4)	106.4(3)
N(2)-Cu(1)-O(3)	104.1(3)	N(7)^{i}-Cu(1)-O(3)	102.6(3)	O(4)-Cu(1)-O(3)	92.4(2)
N(10)^{ii}-Cu(2)-N(9)	109.1(3)	N(10)^{ii}-Cu(2)-N(8)^{i}	124.6(3)	N(9)-Cu(2)-N(8)^{i}	105.7(3)
N(10)^{ii}-Cu(2)-N(1)	114.4(3)	N(9)-Cu(2)-N(1)	94.2(3)	N(8)^{i}-Cu(2)-N(1)	104.3(3)

Symmetry codes: [i] $x-1, y, z$; [ii] $-x+1, -y+1, -z$ for **1**; [i] $-x+3/2, -y+3/2, -z+1$ for **2**; [i] $x, y-1, z$; [ii] $-x, -y+1, -z$ for **3**.

Table 3 Hydrogen bonds for coordination polymers 1~3

D–H···A	d(D-H) / nm	d(H···A) / nm	d(D···A) / nm	∠DHA / (°)
		1		
C(1)–H(1)···O(5)	0.093	0.239	0.326 29	156
C(2)–H(2)···O(7)	0.093	0.230	0.318 86	159
C(4)–H(4)···O(7)	0.093	0.245	0.336 99	172
		2		
O(18)–H(18A)···O(6)	0.096	0.216	0.310 65	167
O(18)–H(18B)···O(19)	0.096	0.188	0.280 18	160
C(10)–H(10)···O(6)	0.093	0.227	0.318 66	170

Continued Table 3

C(13)–H(13)···O(4)	0.093	0.235	0.320 71	154
C(15)–H(15)···O(2)	0.093	0.226	0.310 97	152
		3		
O(14)–H(14A)···O(2)	0.085	0.205	0.286 23	160
O(14)–H(14B)···O(4)	0.085	0.206	0.290 84	177
C(1)–H(1)···O(6)	0.093	0.226	0.306 73	145
C(2)–H(2)···O(9)	0.093	0.241	0.325 61	151
C(6)–H(6)···O(14)	0.093	0.239	0.326 94	157

2　Results and discussion

2.1　Structural description of coordination polymers 1~3

Single-crystal X-ray diffraction analysis demonstrates that coordination compound **1** crystallizes both in $P\bar{1}$ space groups and triclinic crystal system. The asymmetric unit of 1 contains one Cu(Ⅱ) ions, two L_1 ligands, one $Mo_4O_{13}^{2-}$ anion and two lattice water molecules. As illustrated in Fig.1, in coordination polymer **1**, L_1 ligands adopt pyrazolate-like [N-N]-bidentate bridging coordination mode. The Cu(Ⅱ) center (Cu1) is six-coordinated by two nitrogen atoms (N2 and $N2^i$) from triazolyl groups and four oxygen atoms (O1, $O1^i$, $O4^i$ and $O4^{ii}$) from $Mo_4O_{13}^{2-}$. The oxygen atom O(1) coming from $Mo_4O_{13}^{2-}$ anions further links Cu1 atoms. Six-coordinated Cu(Ⅱ) atoms (Cu1) and six-coordinated Mo centers are linked by bidentate L_1 ligands forming binuclear Cu(Ⅱ)-Mo structural units. As depicted in Fig.2(a), the $Mo_4O_{13}^{2-}$ anions are inter-linked via vertical oxygen atoms forming 1D chain structures, which are further joined by Cu(Ⅱ) centers and are arranged into the 2D hybrid metal-organic framework along the crystallographic *c* axis. From side view of the 2D hybrid metal-organic framework (Fig.2(b)), it can be found that the pyridine groups of the bidentate L_1 ligands are not coordinated because of steric hindrance effect, therefore the pyridine groups of L_1 are decorated outside of the 2D coordination framework. Numerous non-classical C–H···O hydrogen bonding interactions (C(1)···O(5) 0.326 29 nm, C(2)···

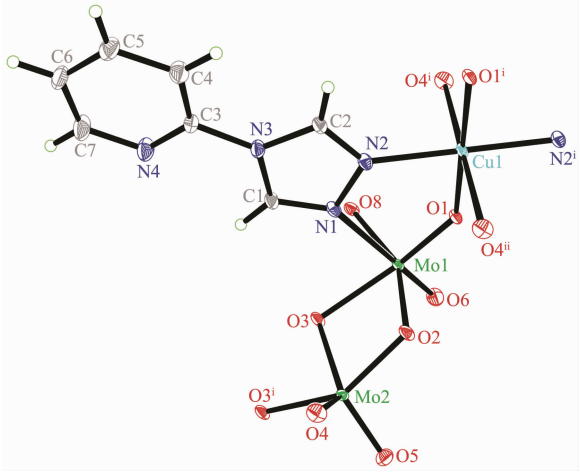

Thermal ellipsoids drawn at 30% probability level; Symmetry codes: ^{i} $x-1, y, z$; ^{ii} $-x+1, -y+1, -z$

Fig.1　Structural unit of **1**

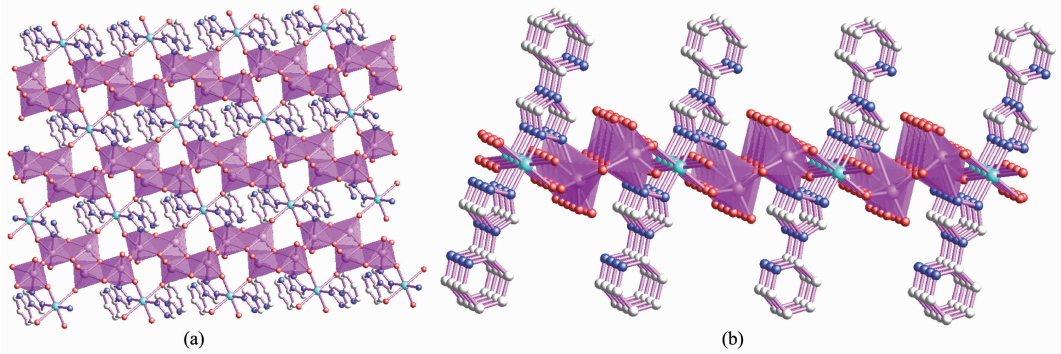

H atoms are omitted for clarity

Fig.2　(a) Two dimensional layer coordination framework of 1 with $Mo_4O_{13}^{2-}$ anions linked by $Cu(L_1)_2$ structural units; (b) Side view of 2D layer coordination framework of **1**

O(7) 0.318 86 nm, C(4)···O(7) 0.336 99 nm) also can be found in the coordination framework of **1**, which also further extend **1** into a 3D supramolecular network.

Coordination polymer **2** crystallizes in *C*2/*c* space groups and monoclinic crystal system. The asymmetric unit of **2** contains 1.5 Cu(Ⅱ) ions (Cu2 and half of Cu1), one HL_2 ligand, one deprotonated L_2^- ligand, one $Mo_4O_{13}^{2-}$ anion, one bridging H_2O molecule (O18) and two lattice H_2O molecules (O19 and O20). As depicted in Fig.3, HL_2 link the neighboring Cu centers (Cu1 and Cu2) through its two nitrogen atoms (N1 and N2) of triazole forming bi-dentate bridging mode. While the deprotonated L_2^- ligands adopt tridentate bridging coordination mode linking Cu1, Cu2 and Cu1^{i} through two triazole nitrogen atoms (N4 and N5) and its one oxygen atom (O15^{i}). The Cu(Ⅱ) center (Cu1) is six-coordinated by two nitrogen atoms (N1 and N4) from triazolyl groups, three oxygen atoms (O1, O12, O15) from $Mo_4O_{13}^{2-}$ and one bridging H_2O molecule (O18). While the Cu(Ⅱ) center (Cu2) is also six-coordinated by four nitrogen atoms (N2, N2^{i}, N5 and N5^{i}) from four triazolyl groups and two bridging water molecule (O18, O18^{i}).

As depicted in Fig.4, the $Mo_4O_{13}^{2-}$ anions are inter-linked via the bridging oxygen atoms (O18), bi-dentate HL_2 and tri-dentate L_2^-, which are further joined by Cu(Ⅱ) centers and are arranged into the unique 3D micro-porous hybrid metal-organic framework along the crystallographic *c* axis. One dimensional micro-

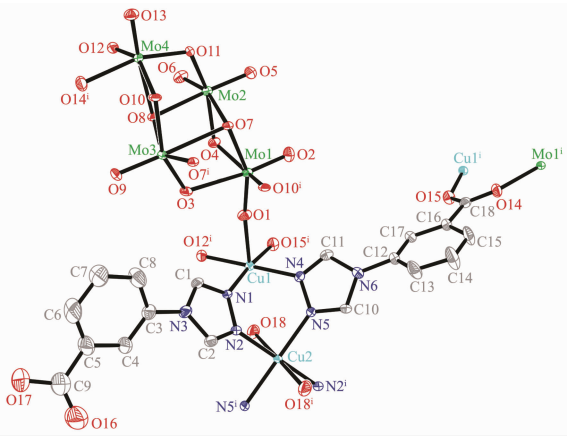

Thermal ellipsoids drawn at 30% probability level; Symmetry codes: ^{i} −*x*+3/2, −*y*+3/2, −*z*+1

Fig.3 Structural unit of **2**

porous channels with 0.479 7(1) nm×0.641 6(1) nm also can be found, in which lattice H_2O molecules are located in the 1D channel. Numerous O−H···O and O−H···O non-classical hydrogen-bonding interactions (O(18)···O(6) 0.310 65 nm, O(18)···O(19) 0.280 18 nm, C(10)···O(6) 0.318 66 nm, C(13)···O(4) 0.320 71 nm, C(15)···O(2) 0.310 97 nm) also can be found in the coordination framework of **2**, which also further stabilize the 3D coordination network of **2**.

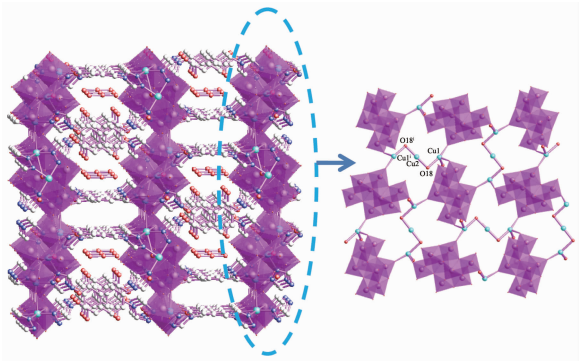

1D micro-porous channels with 0.479 7(1) nm×0.641 6(1) nm can be observed, in which lattice water molecules are located

Fig.4 $Mo_4O_{13}^{2-}$ anions linked by bridging L_2^- forming 3D micro-porous framework of **2**

Coordination polymer **3** crystallizes in $P2_1/c$ space group and monoclinic crystal system. The asymmetric unit of **3** contains two Cu(Ⅰ) ions (Cu1 and Cu2), 1.5 L_3 ligands, one $Mo_4O_{13}^{2-}$ and one lattice H_2O (O14). As depicted in Fig.5, Cu(1) are four-coordinated by two triazole nitrogen atoms (N2 and N7^{i}) and two oxygen atoms (O3 and O4) forming the tetrahedral coordination mode while Cu2 are four-coordination by four triazole nitrogen atoms (N1, N8^{i}, N9 and N10) forming the tetrahedral coordination mode. The L_3 ligands are linked via four neighboring Cu(Ⅱ) ions adopting the tetra-dentate bridging mode.

As depicted in Fig.6(a), the L_3 ligands bridge neighboring Cu(Ⅰ) centers forming 1D double $[Cu_2(L_3)_{1.5}]$ chains. Further the $Mo_4O_{13}^{2-}$ anions are utilized as pillars to link the neighboring 1D double $[Cu_2(L_3)_{1.5}]$ chains forming the 3D POM-based Cu(Ⅰ) hybrid micro-porous framework. It is noted that, as depicted in Fig.6(b), two POM-based 3D micro-porous frameworks self-interpenetrate with each other, which ultimately form two-fold interpenetrating 3D

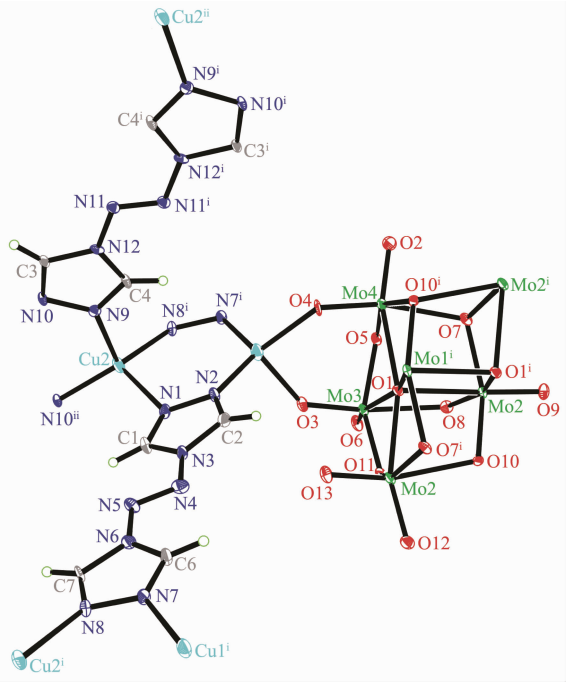

Thermal ellipsoids drawn at 30% probability level; Symmetry codes: [i] x, $y-1$, z; [ii] $-x$, $-y+1$, $-z$

Fig.5　Structural unit of **3**

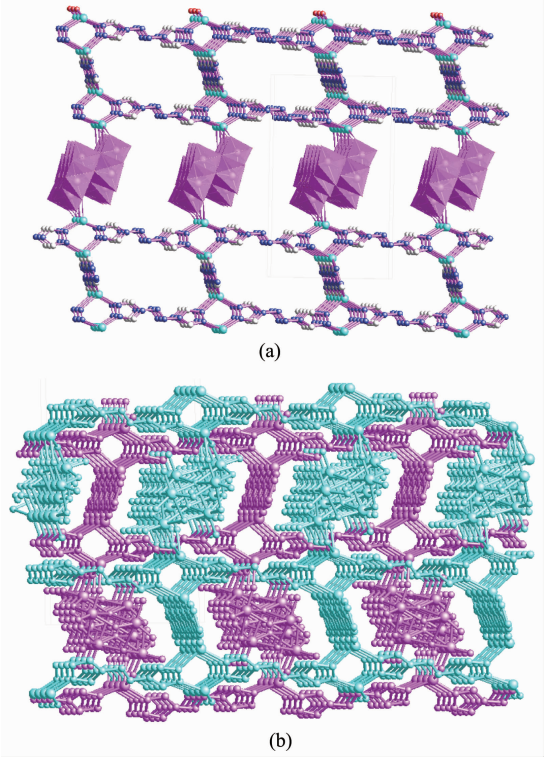

Fig.6　(a) $Mo_4O_{13}^{2-}$ anions used as pillars to link the neighboring 1D double $[Cu_2(L_3)_{1.5}]$ chains forming 3D micro-porous framework; (b) Two-fold interpenetrating 3D coordination framework of **3** viewed along the a-axis direction

coordination framework of **3** viewed along the a-axis direction. The C–H⋯O, N–H⋯O and O–H⋯N hydrogen bonding interactions (O(14)⋯O(2) 0.286 23 nm, O(14)⋯O(4) 0.290 84 nm, C(1)⋯O(6) 0.306 73 nm, C(2)⋯O(9) 0.325 61 nm, C(6)⋯O(14) 0.326 94 nm) can be found, which also further stabilize the 3D hybrid framework of **3** (Table 3)[20].

2.2　Powder X-ray diffraction (PXRD) and FT-IR characterizations

PXRD patterns of coordination compounds **1**~**3** were also determined at ambient temperature to verify the phase purity. As depicted in Fig.7, the experimental patterns positions were well consistent with those of the theoretical patterns, demonstrating the as-

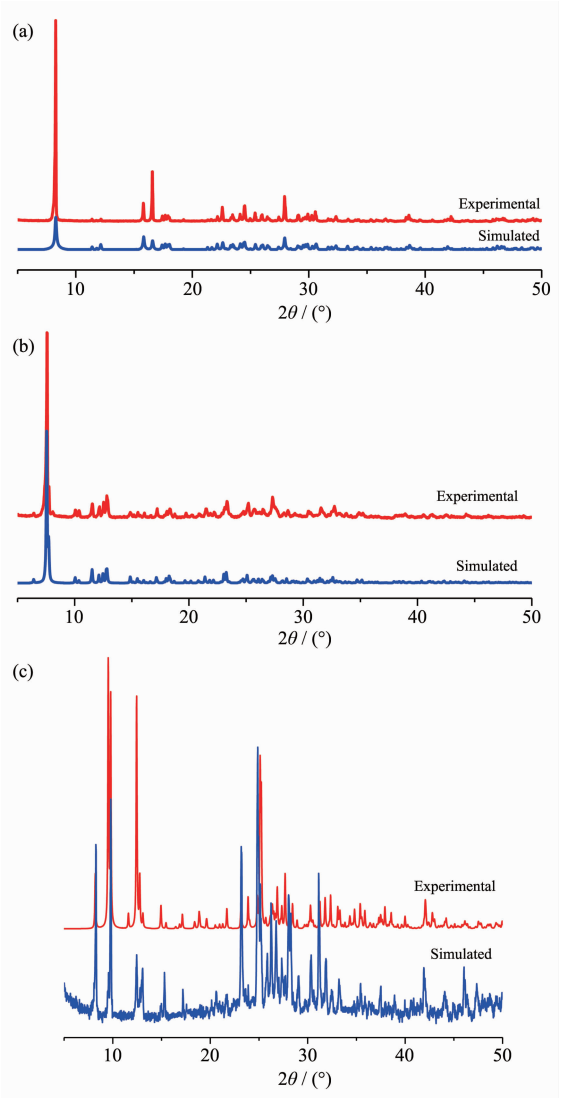

Fig.7　Powder X-ray patterns for coordination framework (a) **1**, (b) **2** and (c) **3** confirming purities of the bulky samples

synthesized samples **1**~**3** are pure phases. The slight differences in reflection intensities between experimental and theoretical PXRD patterns can be ascribed to the crystal orientation variation of the powder samples.

In coordination polymers **1**~**3**, the FT-IR bands at 912, 813 cm^{-1} for **1**, 902, 820 cm^{-1} for **2** and 922, 804 cm^{-1} for **3** can be assigned to ν(Mo-O) and ν(Mo-O-Mo). FT-IR spectra also demonstrated classical absorption bands for triazole moieties of L. The bands around *ca.* 3 100 cm^{-1} and bands located at 1 100~1 300 cm^{-1} should be correlated with ν(C-H) and ν(C-N) or ν(N-N) vibrations of triazole moieties. The triazole out of plane ring absorption is also found at around 600 cm^{-1} (568 cm^{-1} for **1**, 552 cm^{-1} for **2** and 615 cm^{-1} for **3**)[21].

2.2 Photo-catalytic capability for organic dyes by coordination polymers 1~3

As it known to us, large numbers of commercial organic dyes are devoted to our personal life, however, they are also carcinogenic and toxic to us. Therefore how to rational utilize and purify the waste water can be the burning question to solve. Some reported about coordination polymers can show excellent photo-catalytic capability in the organic dyes degradation through the UV irradiation method[22]. To determine the catalytic capability of coordination polymers **1**~**3** for dye degradation, three commercial available common organic dyes RhB, MB and MO have been utilized for the photo-catalytic experiments.

The photo-catalytic activities of coordination polymers **1**~**3** in three different dye solutions are depicted in Fig.8~10, respectively. The variation trend of the concentration ratios of dyes (C_t/C_0) against time (min) for coordination polymers **1**~**3** were plotted, where C_0 is the initial concentration of dyes after stirred in the dark environment for 20 minutes. As depicted in Fig.8, coordination polymer **1** showed remarkable photo-catalytic capacity for the two organic dyes MO and RhB, and could be almost fully degraded (95.8% for RhB, and 97.5% for MO) in 70 min. As depicted in Fig.9, coordination polymer **2** also showed photo-catalytic capacity for the three organic dyes, and could be almost totally degraded (91.1% for MB, 98.6% for RhB and 99.7% for MO) in nearly 70 min. As depicted in Fig.10, coordination polymer **3** showed remarkable photo-catalytic capacity for two organic dyes MO and RhB, and could be nearly

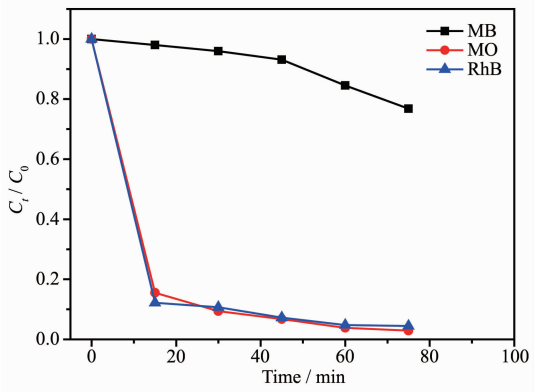

Fig.8 Plot of concentration ratios (C_t/C_0) against irradiation time of MB, RhB and MO degraded by coordination polymer **1**

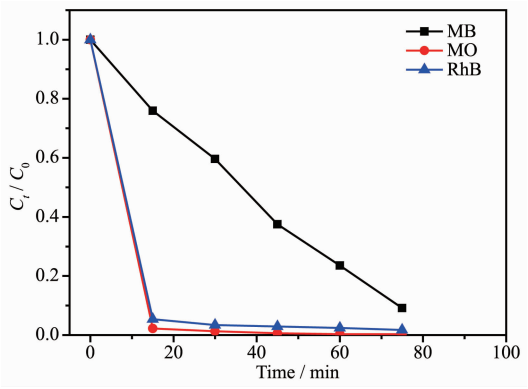

Fig.9 Plot of concentration ratios (C_t/C_0) against irradiation time of MB, RhB and MO degraded by coordination polymer **2**

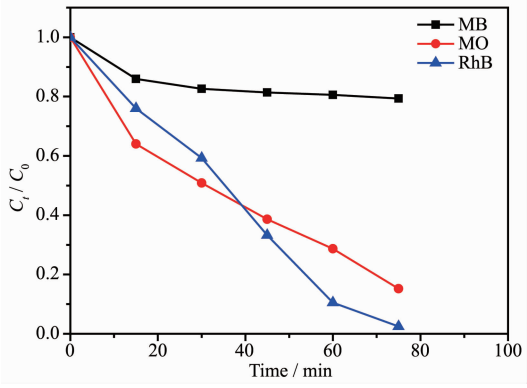

Fig.10 Plot of concentration ratios (C_t/C_0) against irradiation time of MB, RhB and MO degraded by coordination polymer **3**

degraded completely (97.9% for RhB and 84.1% for MO) in 70 min. The experiment results demonstrate that all the coordination polymers **1**~**3** also could be excellent candidates in the photo-catalytic degradation of some organic dyes.

With a view to the coordination environment, the types of the central metal ions and the coordinated mode of the ligand have significant influence on the photocatalytic activities. As described in the previous literature[21], during the photocatalytic process of the POM-based hybrid coordination polymers, UV-Vis light can induce POM/organic ligands to produce oxygen and/or nitrogen-metal charge transfer by promoting an electron from the highest occupied molecular orbital (HOMO) to the lowest unoccupied molecular orbital (LUMO). The HOMO strongly demands one electron to return to its stable state. Thus, one electron is captured from H_2O molecules, which are oxygenated into the ·OH active species, which should further decompose certain organic dyes and effectively complete the photo-catalytic experiment[23-27].

3 Conclusions

In summary, under hydrothermal conditions, three novel polyoxometalate (POM)-based Cu(Ⅱ) and Cu(Ⅰ) hybrid materials with multi-dentate mono- and bis-triazole derivatives, namely $\{[Cu(L_1)_2(Mo_4O_{13})]\cdot 2H_2O\}_n$ (**1**), $\{[Cu_{1.5}(L_2)(HL_2)(H_2O)(Mo_4O_{13})]\cdot 2H_2O\}_n$ (**2**), $\{[Cu_2(L_3)_{1.5}(Mo_4O_{13})]\cdot H_2O\}_n$ (**3**) have been designed and synthesized. In **1**, the $Mo_4O_{13}^{2-}$ anions and Cu(Ⅱ)centers are inter-linked by bidentate L_1, which are arranged into the 2D hybrid metal-organic framework. In **2**, the $Mo_4O_{13}^{2-}$ anions and Cu(Ⅱ) centers are inter-linked via bridging aqua atoms (O18), bi-dentate HL_2 and tri-dentate L_2^-, which are arranged into the 3D micro-porous hybrid metal-organic framework. In **3**, the L_3 ligands bridge neighboring Cu(Ⅰ) centers and $Mo_4O_{13}^{2-}$ anions, which ultimately form the two-fold interpenetrating 3D coordination framework of **3**. Photocatalytic activities for decomposition of different organic dyes RhB, MB and MO have been investigated, and the results indicate that **1**~**3** are good candidates for photocatalytic degradation of the organic dyes. The experiment result also demonstrates that great potential in the construction of the novel POM-based hybrid metal organic frameworks employing different multi-dentate mono- and bis-triazole derivatives and versatile polyoxometalate (POM)-based building blocks. On the basis of this work, further preparation, structural analyses and functional properties investigations of the POM-based hybrid coordination polymers utilizing the versatile building blocks are also under way in our laboratory.

References:

[1] (a)Banerjee R, Phan A, Wang B, et al. *Science*, **2008**,**319**:939-943
(b)Zhu P P, Sun L J, Sheng N, et al. *Cryst. Growth Des.*, **2016**,**16**:3215-3223
(c)Bijelic A, Rompel A. *Acc. Chem. Res.*, **2017**,**50**:1441-1448

[2] (a)Anjass M H, Kastner K, Nagele F, et al. *Angew. Chem. Int. Ed.*, **2017**,**56**:14749-14752
(b)He W W, Li S L, Zang H Y, et al. *Coord. Chem. Rev.*, **2014**,**279**:141-160
(c)Wang X, Zhang Q, Nam C, et al. *Angew. Chem. Int. Ed.*, **2017**,**56**:11826-11829

[3] (a)Yi X F, Izarova N V, Stuckart M, et al. *J. Am. Chem. Soc.*, **2017**,**139**:14501-14510
(b)Liu Y P, Zhao S F, Guo S X, et al. *J. Am. Chem. Soc.*, **2016**,**138**:2617-2628

[4] (a)Yu Y, Zhang Q, Buscaglia J M. *Analyst*, **2016**,**141**:4424-4431
(b)Zhang Q, Kaisti M, Prabhu A, et al. *Electrochim. Acta*, **2017**,**261**:256-264
(c)Zhang Z M, Duan X P, Yao S, et al. *Chem. Sci.*, **2016**,**7**:4220-4229
(d)Liu R J, Zhang G J, Cao H B, et al. *Energy Environ. Sci.*, **2016**,**9**:1012-1023

[5] (a)Kaisti M, Zhang Q, Levon K, et al. *Sens. Actuators B: Chem.*, **2017**,**241**:321-326
(b)Yu Y, Zhang Q, Wang Y, et al. *Analyst*, **2016**,**141**:5607-5617
(c)Fu H, Qin C, Lu Y, et al. *Angew. Chem. Int. Ed.*, **2012**, **51**:7985-7989
(d)Genovese M, Lian K. *J. Mater. Chem. A*, **2017**,**5**:3939-3947

[6] (a)Wei X, Panindre P, Zhang Q, et al. *ACS Sens.*, **2016**,**1**:862-865

(b)Zhu S L, Xu X, Ou S, et al. *Inorg. Chem.*, **2016**,**55**:7295-7300

(c)Xin X, Tian X R, Yu H T, et al. *Inorg. Chem.*, **2018**,**57**:11474-11481

(d)Li X X, Zhang L J, Cui C Y, et al. *Inorg. Chem.*, **2018**, **57**:10323-10330

[7] (a)Chen L Y, Luque R, Li Y W, et al. *Chem. Soc. Rev.*, **2017**, **46**:4614-4630

(b)Bennett J W, Bjorklund J L, Forbes T Z, et al. *Inorg. Chem.*, **2017**,**56**:13014-13028

(c)Lysenko A B, Bondar O A, Senchyk G A, et al. *Inorg. Chem.*, **2018**,**57**:6076-6083

[8] Zhu P P, Sun L J, Sheng N, et al. *Cryst. Growth Des.*, **2016**, **16**:3215-3223

[9] Li X X, Wang Y X, Wang R H, et al. *Angew. Chem. Int. Ed.*, **2016**,**55**:6462-6466

[10]Haasnoot J G. *Coord. Chem. Rev.*, **2000**,**200-202**:131-185

[11]Li X X, Xu H Y, Kong F Z, et al. *Angew. Chem. Int. Ed.*, **2013**,**52**:13769-13773

[12]Zhu P P, Sheng N, Li M T, et al. *J. Mater. Chem. A*, **2017**,**5**:17920-17925

[13](a)Ding B, Yi L, Cheng P, et al. *Inorg. Chem.*, **2006**,**45**:5799-5803

(b)Ding B, Liu S X, Cheng Y, et al. *Inorg. Chem.*, **2016**,**55**:4391-4402

[14]Liu J Y, Wang Q, Zhang L J, et al. *Inorg. Chem.*, **2014**,**53**:5972-5985

[15]Wang Y, Yuan B, Xu Y Y, et al. *Chem. Eur. J.*, **2015**,**21**:2107-2116

[16](a)Cheng Y, Wu J, Guo C, et al. *J. Mater. Chem. B*, **2017**,**5**:2524-2535

(b)Wang X R, Du J, Huang Z, et al. *J. Mater. Chem. B*, **2018**,**6**:4569-4574

[17](a)Gusev A N, Nemec I, Herchel R, et al. *Dalton Trans.*, **2014**,**43**:7153-7163

(b)Naik A D, Marchand-Brynaert J, Garcia Y. *Synthesis*, **2008**,**1**:149-154

[18]Sheldrick G M. *SHELXS*-97, *Program for X-ray Crystal Structure Solution*, University of Göttingen, Germany, **1997**.

[19]Sheldrick G M. *SHELXL*-97, *Program for X-ray Crystal Structure Refinement*, University of Göttingen, Germany, **1997**.

[20]Spek A L. *J. Appl. Crystallogr.*, **2003**,**36**:7-13

[21]Senchyk G A, Lysenko A B, Domasevitch K V, et al. *Inorg. Chem.*, **2017**,**56**:12952-12966

[22]Fiher M E. *Am. J. Phys.*, **1964**,**32**:343-345

[23]Wang X L, Gong C H, Zhang J W, et al. *CrystEngComm*, **2015**,**17**:4179-4189

[24](a)Cui J W, An W J, Kristof Van H, et al. *Dalton Trans.*, **2016**,**45**:17474-17484

(b)Jia C, Xie X W, Ge M, et al. *Mater. Sci. Semicond. Process.*, **2015**,**36**:71-77

[25]Dolbecq A, Mialane P, Keita B, et al. *J. Mater. Chem.*, **2012**,**22**:24509-24521

[26](a)Zhang Q, Khajo A, Sai T, et al. *J. Phys. Chem. A*, **2012**, **116**:7629-7635

(b)Hu J M, Blatov V A, Yu B Y, et al. *Dalton Trans.*, **2016**, **45**:2426-2429

[27]Meng X M, Fan C B, Bi C F, et al. *CrystEngComm*, **2016**, **18**:2901-2912